Dynamic vs. apparent Redfield ratio in the oceans: A case for 3D-models

Ernst Maier-Reimer

Max Planck-Institut für Meteorologie, Hamburg, Germany

Abstract

A three-dimensional model of global biogeochemical cycles (HAMOCC3) is used to discuss potential explanations for apparent observed deviations from a basin-wide Redfield ratio. Two examples are given in which model information can be taken to close the gaps of incomplete measurements or data analyses. A third example illustrates how the apparent covariation between phosphate and alkalinity is created by the circulation.

1. Introduction

The observation that the remnants of remineralization processes are highly correlated in the deep ocean (Redfield, 1934; Takahashi et al., 1985) has strongly influenced our ideas of how the global biogeochemical flux pump operates. Although it is unlikely that a perfect stoichiometric relationship exists between the elementary constituents even within one species, not to mention between different species (Wynne and Rhee, 1986; Nielsen and Tonseth, 1991), the deviations seem to compensate each other in the large scale chemical distributions in the deep sea. In the upper parts of the oceans, however, pronounced deviations from the deep sea chemical ratios are observed. You and Tomczak (1993) discuss the relationship between oxygen and phosphate in the thermocline waters of the Indian Ocean where the ratio apparently is 130:1, compared with the deep sea value of 170:1. Sambrotto et al. (1993) reported substantial deviations from the deep sea ratio of C:N in the seasonal cycle of productivity. In both papers

it is concluded that the concept of a constant Redfield ratio should be questioned and at least revised, if not abandoned all together.

For global modelling studies (cf. Maier-Reimer, 1993), the assumption of a constant Redfield ratio represents an efficient mechanism to reduce the number of free parameters and, thus, to increase the efficiency of any model prediction. In comparing model results with data on local variations of the geochemical relationships, it is then possible to discriminate between different processes that were not subject to measurements. For such purposes, it is not crucial that the model be fully accurate; as long as the basic structures are reproduced qualitatively, a reliable estimate on the order of magnitude of the neglected processes can be achieved. In this note, I discuss how parts of the observed non-Redfield properties may be explained by confining the discussion to restricted problems, neglecting for the present their part in the global flux system.

2. Oxygen to phosphate ratio in the Indian Ocean thermocline

Based on water mass analyses on isopycnal surfaces, You and Tomczak (1993) concluded that thermocline waters in the Indian Ocean seem to be characterised by a phosphate to oxygen Redfield ratio of 1:130, whereas in the deep Pacific and Indian Oceans an almost linear relationship is observed with a slope of 170 moles of oxygen per mole of phosphate. The authors briefly mentioned the potential existence of diapycnal mixing, but ignored it within the framework of their analysis. Motivated by this finding, Anderson and Sarmiento (1995) performed experiments with their nutrient cycling model (Najjar et al., 1992) with different assumptions on the $P:O_2$ Redfield ratio. In the standard experiment they used a constant value of 170. In a second experiment, they prescribed explicitly a ratio of 138 in order better to match the observations. That paper illustrates clearly that a model output does not necessarily improve when the model is constrained by additional data. The failure of the second experiment to yield any substantial improvement of the reproduction of tracer distributions indicates that some important process which determines the observed slope is overlooked.

A plausible explanation could be that different size classes of the organic debris have different Redfield ratios. Such an hypothesis completely neglects the effects of the ongoing diapycnal mixing of the tracers which have quite different boundary conditions at the sea surface. In this section, I discuss the evolution of an apparent basin-wide Redfield ratio from bottom to top in a three dimensional model of geochemical cycling in the ocean (HAMOCC3; Maier-Reimer, 1993; abbreviated here as PTD).

The structure of surface phosphate distribution as a result of the export production (Maier-Reimer, 1993, fig. 2a) is governed by simple Michaelis-Menten type of kinetics. The soft tissue products are released downwards with a penetration profile proportional to $z^{-0.8}$ (Suess, 1980). During remineralization, a constant Redfield ratio of 1:172 is assumed. The same ratio is applied for the production
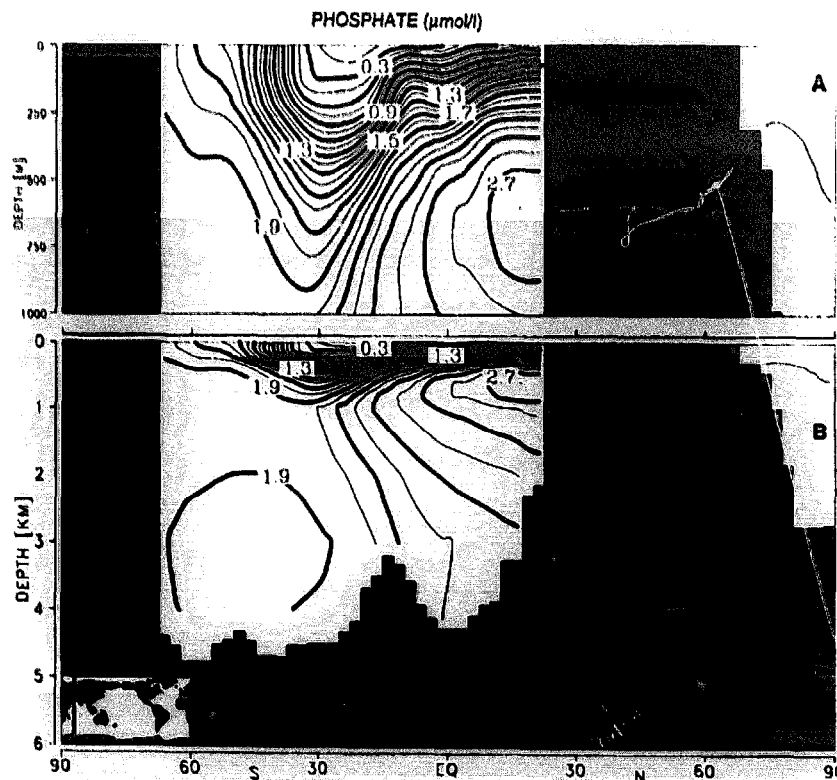

PHOSPHATE (μmol/l)

Fig. 1. Distribution of phosphate along a section in the western Indian Ocean. (A) represents the upper 1000 m in detail; (B) represents the full depth of the Ocean. The inset shows the position of the transect.

of oxygen at the sea surface by photosynthesis. There is a resulting covariation of O_2 with PO_4 to a depth of 3km (Maier-Reimer, 1993, fig. 5)

The thermohaline circulation in the Indian Ocean is characterised by a basin-wide upwelling which is fed from Antarctic bottom water and a branch of North Atlantic deep water. It is balanced by an upper layer outflow to the south, yielding a southward heat transport over the entire extent of the Ocean. The mixing of surface properties is enhanced by the strong seasonal fluctuations that are driven by Monsoon cycles.

The simulated phosphate distribution along a section in the western Indian Ocean is illustrated in Fig. 1. The absolute maximum of 2.81 μmol/kg at a depth of 600 m evolves from a balance between the prevailing upwelling flux, continual remineralization, and blending with surface waters. For radiocarbon (Fig. 2), the internal sink by decay acts on a much longer time scale, the absolute minimum of −178‰ being at a depth of 2 km.

The covariation of oxygen and phosphate in the Indian Ocean, for a reduced set of grid points (every

second in longitude) is illustrated in Fig. 3. The surface values are denoted by " + " and subsurface values warmer than 8°C are labelled " ˚ ", and those colder than 8°C by " − ". The subsurface values are restricted to the domain north of 30°S since in the mid-latitude subduction zone the water becomes mixed with Antarctic water (You and Tomczak, 1993, based their study on the domain up to 40°S, but in the southern part the data were extremely sparse). The surface covariation of oxygen with phosphate from the model is dominated by the correlation between warm waters that are poor in oxygen and phosphate, and the cold Antarctic water where both tracers have high concentrations. Obviously, the scatter at the surface is almost perpendicular to the assumed Redfield ratio. However, along the equator, moderately high phosphate concentrations are connected with low oxygen and thus form a separate cluster. The straight lines denote constant values of:

$$PO_4^* = PO_4 + O_2/172 - 1.95 \,\mu mol/l$$

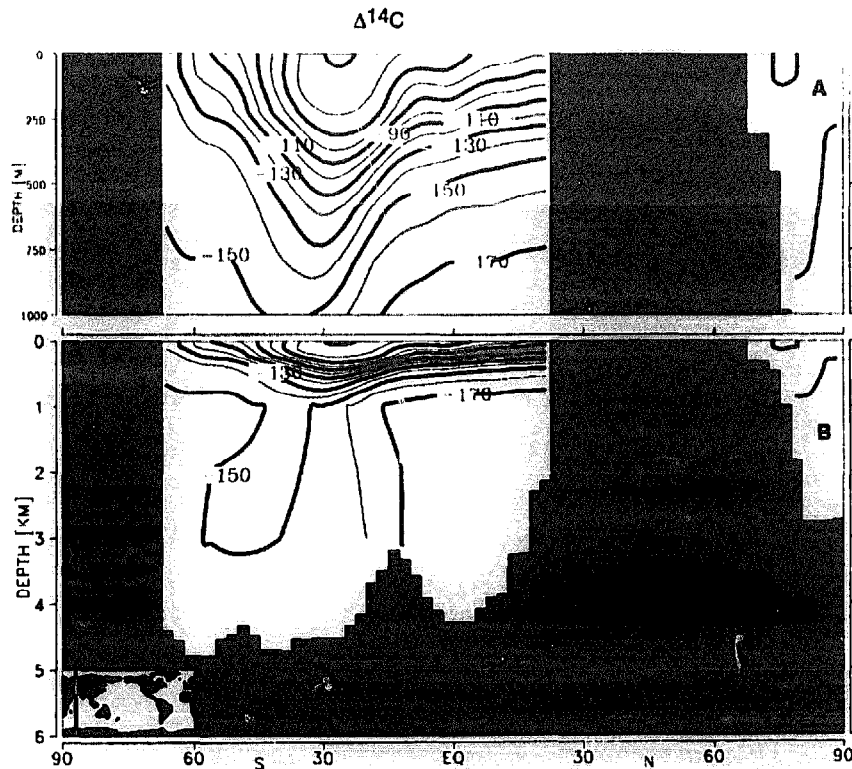(Blanton et al., 1991), a modified expression of preformed phosphate which, under the assumption of

Fig. 2. Distribution of $\Delta^{14}C$ along a section in the western Indian Ocean. (A), (B) and inset as Fig. 1.

a perfect Redfield ratio, should be a conservative tracer in the deep sea. It varies in the deep ocean between 0.7 in the deep Northern Atlantic and 1.7 in the Weddell Sea.

The circulation in this diagram is counter clockwise. The water enters the deep Indian Ocean at $(O_2, PO_4) = (200, 2)$. During its northern flow with upwelling it collects the products of remineralization processes, i.e. it undergoes phosphate enrichment and oxygen depletion. From the tropical surface it joins the Antarctic Circumpolar Current (ACC) partly by subduction in the Ekman drift convergence and partly by the Agulhas current which is persistently retroflected in the model. Part of the variation in the deep ocean can be explained by blending with North Atlantic Deep Water (NADW) which has a PO_4^* of 0.7. In shallower depths, the variation is mostly due to mixing with tropical surface properties. The thick regression line in Fig. 3 for subsurface thermocline water is given by:
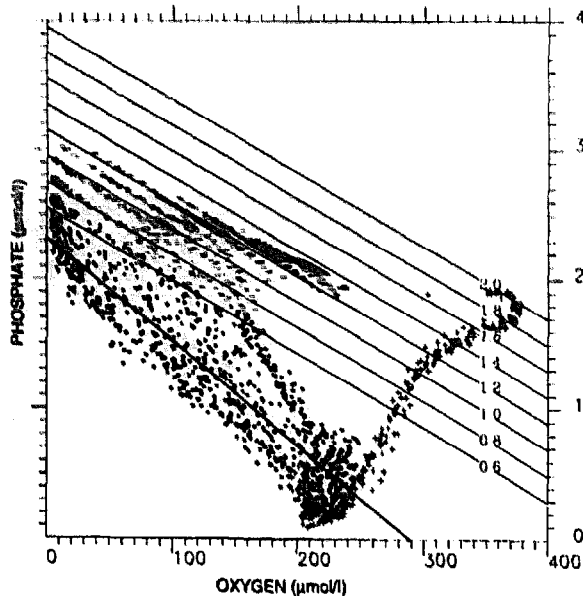
$$PO_4 = 2.31 - O_2/125$$

Fig. 3. Covariation of O_2 and PO_4 in the Indian Ocean. The surface values are denoted by " + ", subsurface values warmer than 8°C are labelled " * ", and " – " denotes values colder than 8°C. The subsurface values are restricted to the domain north of 30°S. The circulation in this diagram acts counterclockwise. The thinner straight lines represent constant values of: $PO_4^* \approx PO_4 + O_2/172 - 1.95$ μmol/l (see text, p. 115); the thicker straight line represents: $PO_4 = 2.31 - O_2/125$ (see text, p. 116).

The computed slope depends on the southern boundary of the domain of analysis, i.e. the probability that the water is blended with Antarctic surface water: for 20°S it is at 109, whereas for the equator it is at 95. It depends also on the temperature range which has to be taken into account. When water bodies with lower temperature are included in the regression, the slope becomes steeper.

3. Carbon and nutrient fixation in organic production

Sambrotto et al. (1993) discussed the covariation between changes of dissolved inorganic carbon and of nitrate in surface waters at several stations for time intervals from weeks to months. After a careful examination of the effects of evaporation/precipitation and formation of calcareous shells by correcting for variations in salinity and alkalinity, they concluded that the C/N ratio in marine production should be much higher than thought before. They suggest, therefore, that "the growth of ocean plankton has been underestimated as a sink for atmospheric CO_2". Without going into the discrimination of potentially different roles of this conjecture for natural and anthropogenic CO_2, nor into the problems that may stem from the coexistence of "new" (i.e. nitrate consuming) and "regenerated" (i.e. consuming other nitrogen compounds like ammonia) production, I discuss in this section the potential role of air-to-sea transports of CO_2 on the covariation with phosphate. This transport is difficult to estimate from observations since pCO_2 and the effective gas exchange coefficient are hard to measure. From measurements, one should compute the flux, F, from:

$$F = k\delta pCO_2$$

where k is the gas exchange coefficient and δpCO_2 is the difference in partial pressure between ocean and atmosphere. From experiments with the PTD model (Maier-Reimer, 1993), however, it was confirmed that the flux is determined primarily by divergences in the ocean and the partial pressure establishes to first order approximation according to:

$$\delta pCO_2 = F/k$$

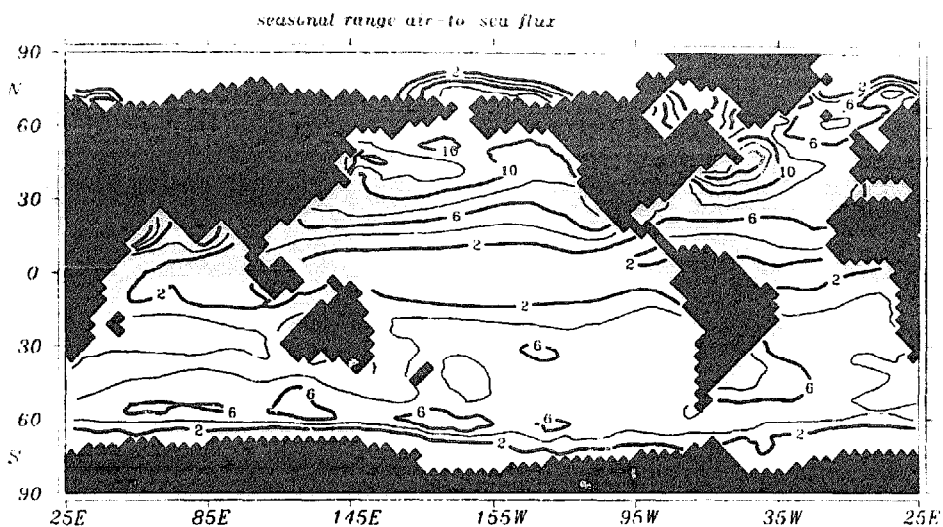Experiments with different formulations of k gave indeed quite different distributions of pCO_2, but

Fig. 4. Seasonal range of global variations of ΣCO_2 induced by gas exchange with the atmosphere. The contour interval is 2.0 μmol l^{-1} month^{-1}.

similar distributions of the net air-to-sea flux of CO_2. Within the framework of a model, the estimate of the relative importance of the gas transfer is, thus, more robust than from observations. The divergences in the ocean are caused by production and currents. The pCO_2 is additionally influenced by temperature. The seasonal effects of production and temperature on the pCO_2 are opposite in sign in many parts of the ocean. In spring, the rising temperature tends to cause CO_2 release, while rising production tends to

remove CO_2. It depends on local conditions which one of the two effects dominates. In high latitudes, the switch from unfavourable to favourable conditions for growth occurs rather quickly (Takahashi et al., 1993) and the production effect overrides the thermodynamic effect (in the present form of the PTD model, this feature is not reproduced).

A model of the annual mean δpCO_2 between ocean and atmosphere is characterised by a strong high in the Equatorial Pacific and moderate lows in
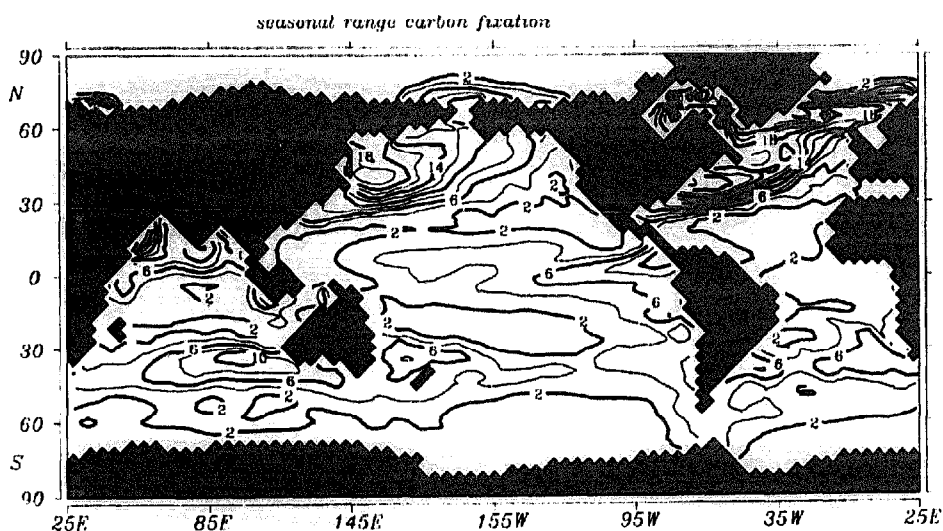

Fig. 5. Seasonal range of global variations of ΣCO_2 induced by fixation into organic material. The contour interval is 2.0 μmol l^{-1} month^{-1}.
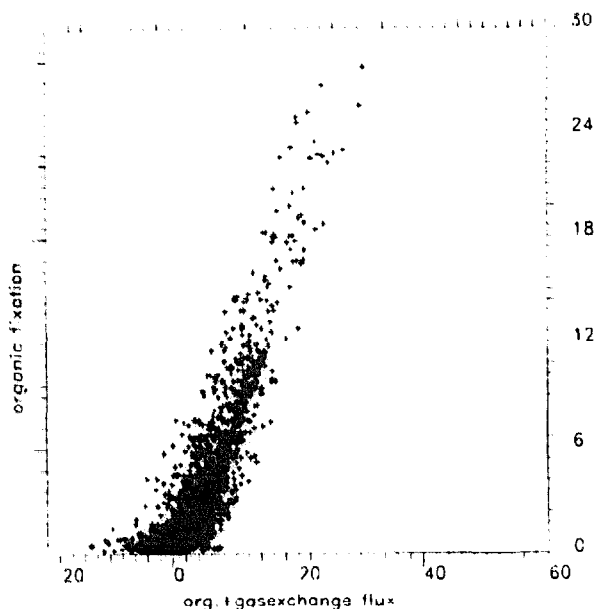
Fig. 6. Covariation of organic fixation and total carbon variations (μmol l^{-1} month^{-1}) that are not linked with variations of salinity and alkalinity.

high latitudes, especially in the Northern Atlantic (Maier-Reimer, 1993, fig. 11). Below compact sea ice, the gas exchange is blocked and the values are set to zero. The seasonal range of effective carbon fluxes is shown in Fig. 4. The range is below 2.0 μmol l^{-1} month^{-1} almost everywhere along the equator and increases towards higher latitudes. The absolute maximum is near Labrador with a range of 12 μmol l^{-1} month^{-1}. The seasonal range of carbon fixation (Fig. 5) looks rather similar and the numbers are comparable. With the assumption of a perfect Redfield ratio, this figure can also be taken as phosphate consumption. For the apparent variations in the sea water chemistry, the phasing between the two fluxes is crucial. The scatter between the sum of the fluxes and the flux by carbon fixation for the Atlantic portion of the model is illustrated in Fig. 6. There are a few points where the total flux is determined almost exclusively by the high productivity. At low productivities the total flux has both signs. The whole cluster appears to be correlated in a way that total carbon variations are higher than the consumption in organic production. This is due to the parallel nature of the individual fluxes: in summer, the water becomes depleted in CO_2 (ΣCO_2) by carbon fixation in organic material, and also by

exchange to the atmosphere through the temperature induced pCO_2.

4. Alkalinity variations

Alkalinity is the key control variable that determines carbon fluxes across the air-to-sea interface. Like salinity, it is modified at the sea surface by precipitation and evaporation. (Since the overall variations are relatively small compared with the mean value, this mechanism has a stronger impact on alkalinity than on nutrients or DIC). It is also increased by the production of organic (soft tissue) material due to the incorporation of nitrate, and it is decreased by production of calcareous structures, such as coccoliths. During the remineralization of soft tissue and dissolution of calcite, the reverse changes occur. The strong regional variability of sediment trap data (Tsunogai and Noriki, 1991) makes a global estimate of the relative amounts of the pumps rather uncertain. From the overall gradients of DIC and alkalinity a mean C_{org}:$CaCO_3$ relationship of about 4.0 can be derived (Broecker and Peng, 1982), but this estimate is hampered by the uncertainty of thermodynamic influences on DIC. The model yields a global mean ratio of 6.0 and the regional distribution is illustrated in Maier-Reimer (1993, fig. 1d).

The differences of the source/sink terms make the evaluation of scatter diagrams rather problematic. The covariation between alkalinity (normalised with salinity) and phosphate below 1500 m from the model and from the GEOSECS data (Bainbridge, 1980; Craig et al., 1981) looks like the manifestation of a new Redfield relationship (Fig. 7a), but the sign of the correlation is opposite to the assumed Redfield mechanism which links release of phosphate with consumption of alkalinity. Obviously, the scatter displays primarily the mixing line between North Atlantic deep water from which both are exported and Pacific deep water where both are enriched. The model has a constant set-up of approx. 50 μmol kg^{-1} in alkalinity, but the slope of the regression line is realistically simulated.

The effect of calcite producers on the distribution of alkalinity is easily derived from an experiment with doubled potential for calcite formation and the corresponding PO_4 vs alkalinity scatter from such a
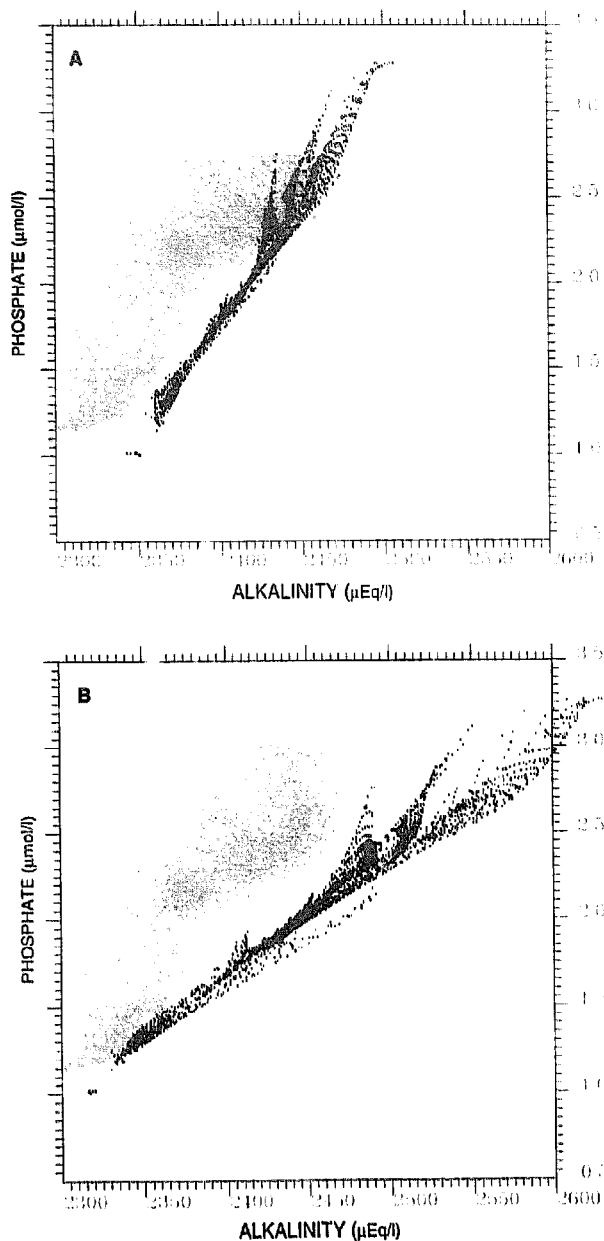
ALKALINITY (μEq/l)

ALKALINITY (μEq/l)

Fig. 7. a. Covariation of alkalinity (salinity normalized) and PO_4 below 1500 m: GEOSECS data (grey scatter) and model values (dark scatter). The three branches of the model scatter represent the differences between the horizons 2, 3, and 4 km, the highest values lying in the 2 km layer. b. As (a), but with doubled rate of calcite formation.

run is illustrated in Fig. 7b. The overall variation of alkalinity is also doubled and the depletion in the northern Atlantic is enhanced by about 20 μmol kg^{-1}. The comparison between the results shown in Fig. 7a,b indicates that with the assumed penetration

profiles, a global mean rain ratio of 6:1 for $C_{org}:CaCO_3$ is more likely than the ratio 3:1.

The other changes of simulated marine chemistry from the doubling experiment are rather small. With given inventories of alkalinity and ΣCO_2, the atmospheric pCO_2 is raised by approx. 18 ppm. As the doubling acts uniformly, the changes in the structure of air-to-sea flux of CO_2 are rather small. The increased export of alkalinity from Atlantic to Pacific yields a slight decrease in depth of the lysocline in the Atlantic and a deepening of the lysocline in the Pacific by approx. 1 km.

5. Conclusion

It is shown that some observed discrepancies to a globally constant Redfield ratio may be explained by physical processes like mixing and gas transfer. Although far from perfect, models can be taken as a tool for the interpretation of original data. However, modellers should be extremely careful when manipulating chemically active components of Redfield ratios in order to explain observed apparent variations.

Acknowledgements

References

Anderson, L.A. and Sarmiento, J.L., 1995. Global ocean phosphate and oxygen simulations. Global Biogeochem. Cycles, in press.

Bainbridge, A., 1980. 1981 GEOSECS Atlantic Expedition; sections and profiles. Natl. Sci. Found., Washington.

Blanton, S., Takahashi, T., Smethie, W. and Ostlund, G., 1991. Radiocarbon decay and oxygen utilization in the deep Atlantic Ocean. Global Biogeochem. Cycles, 5: 87–117.

Broecker, W.S. and Peng, T.H., 1982. Tracers in the Sea. Eldigio Presss, Palisades, NY.

Craig, H., Broecker, W.S. and Spencer, D., 1981. GEOSECS Pacific Expedition; sections and profiles. Natl. Sci. Found., Washington.

Maier-Reimer, E., 1993. Geochemical cycles in an ocean general circulation model. Preindustrial tracer distributions. Global Biogeochem. Cycles, 7: 645–677.

Najjar, R.G., Sarmiento, J.L. and Toggweiler, J.R., 1992. Downward transport and fate of organic matter in the ocean: Simulations with a general circulation model. Global Biogeochem. Cycles, 6: 45–76.

Nielsen, M.V. and Tonseth, C.P., 1991. Temperature and salinity effect on growth and chemical composition of *Gyrodinium aureolum* Hulburt in culture. J. Plankton Res., 13: 389–398.

Redfield, A.C., 1934. On the proportion of organic derivatives in sea water and their relation to the composition of plankton. In: James Johnstone Memorial Volume. Univ. Liverpool, pp. 176–192.

Sambrotto, R.N., Savidge, G., Robinson, C., Boyd, P., Takahashi, T., Karl, D.M., Langdon, C., Chipman, D., Marra, J. and Codispoti, L., 1993. Elevated consumption of carbon relative to nitrogen in the surface ocean. Nature, 363: 248–250.

Suess, E., 1980. Particulate organic carbon flux in the oceans— surface productivity and oxygen utilization. Nature, 288: 260–263.

Takahashi, T., Broecker, W.S. and Langer, S., 1985. Redfield ratio estimates based on chemical data from isopycnal surfaces. J. Geophys. Res., 90: 5907–5924.

Takahashi, T., Olafson, J., Goddard, J.G., Chipman, D.W. and Sutherland, S.C., 1993. Seasonal variations of CO_2 and nutrients in the high-latitude surface oceans: A comparative study. Global Biogeochem. Cycles, 7: 843–878.

Tsunogai, S. and Noriki, S., 1991. Particulate fluxes of carbonate and organic carbon in the ocean. Is the marine biological activity working as a sink of the atmospheric carbon? Tellus, 43B: 256–266.

Wynne, D. and Rhee, G.Y., 1986. Effects of light intensity and quality on the relative N and P requirement (the optimum N:P ratio) of marine planktonic algae. J. Plankton Res., 8: 91–103.

You, Y. and Tomczak, M., 1993. Thermocline circulation and ventilation in the Indian Ocean derived from water mass analysis. Deep-Sea Res., 40: 13–56.